40-character title: Lake Chala: 250-ky record of basaltic volcanism

History of scoria-cone eruptions on the eastern shoulder of the Kenya-Tanzania Rift revealed in the 250-ky sediment record of Lake Chala near Mt. Kilimanjaro

Catherine Martin-Jones[a, b]*, Christine Lane[a], Maarten Van Daele[c], Thijs Van der Meeren[b], Christian Wolff[d], Heather Moorhouse[d], Emma Tomlinson[e] and Dirk Verschuren[b]

[a]*Department of Geography, University of Cambridge, Cambridge CB2 3EN, UK*

[b]*Limnology Unit, Department of Biology, Ghent University, B-9000 Gent, Belgium*

[c]*Renard Centre of Marine Geology, Department of Geology, Ghent University, B-9000 Gent, Belgium*

[d]*Lancaster Environment Centre, University of Lancaster, Lancaster LA1 4YQ, UK*

[e]*Department of Geology, Trinity College Dublin, Dublin 2, Ireland*

Abstract

Reconstructions of the timing and frequency of past eruptions are important to assess the propensity for future volcanic activity, yet in volcanic areas such as the East African Rift only piecemeal eruption histories exist. Understanding the volcanic history of scoria cone fields, where eruptions are often infrequent and deposits strongly weathered, is particularly challenging. Here we reconstruct a history of volcanism from scoria cones situated along the eastern shoulders of the Kenya-Tanzania Rift, using a sequence of tephra (volcanic ash) layers preserved in the ~250-ky sediment record of Lake Chala near Mt. Kilimanjaro. Seven visible and two non-visible (crypto-) tephra layers in the Lake Chala sequence are attributed to activity from the Mt. Kilimanjaro (northern Tanzania) and the Chyulu Hills (southern Kenya) volcanic fields, on the basis of their glass chemistry, textural characteristics and known eruption chronology. The Lake Chala record of eruptions from scoria cones in the Chyulu Hills volcanic field confirms geological and historical evidence of its recent activity, and provides first-order age estimates for seven previously unknown eruptions. Long and well-resolved sedimentary records such as that of Lake Chala have significant potential for resolving regional eruption chronologies spanning hundreds of thousands of years.

*corresponding author: C Martin-Jones, martinjonescatherine@gmail.com

Keywords: East African Rift; tephrochronology; Lake Chala; Mt. Kilimanjaro volcanic field; Chyulu Hills volcanic field; tephra glass geochemistry

1. Introduction

1.1. Volcanism in East Africa

The East African Rift system (EARS) marks one of Earth's best-preserved continental rift systems - a fascinating natural laboratory in which to study compositionally diverse volcanism and wide-ranging volcanic hazards. Volcanism in Kenya and Tanzania tracks the eastern branch of the EARS, where rifting was initiated ~35 Ma in the Lokichar Basin of northern Kenya (Fig. 1; Macgregor, 2015). Twenty-one volcanoes in Kenya and 10 in Tanzania are believed to have been active during the Holocene, on the basis of their morphology and evidence of historical or recent geological activity (Global Volcanism Program*,* 2013). Whilst there is little data on past volcanism, an increasing number of volcanological, archaeological and palaeoenvironmental studies are beginning to compile and date eruptive deposits preserved both in terrestrial and lake-sediment sequences throughout East Africa (*e.g*. Poppe *et al.,* 2016; Campisano *et al.,* 2017; Fontijn *et al.,* 2018, McNamara *et al.,* 2018). These tephrostratigraphic studies indicate that many volcanoes of the Kenya-Tanzania Rift have erupted explosively during the Holocene, depositing ash over hundreds of kilometres (Fontijn et al., 2010, 2018; Martin-Jones *et al.,* 2017; 2018; Lane *et al.,* 2018; McNamara *et al.,* 2018).

During the Late Pleistocene, volcanism within the EARS has been strongly bimodal. Silicic eruptions from central volcanoes occurred alongside less abundant basaltic eruptions from fissure vents – whilst intermediate compositions have been comparatively rare (Baker, 1987; Williams, 1984; MacDonald, 1995; McDoughall and Brown, 2009). The volcanoes of the Kenya-Tanzania Rift have been divided into northern and southern sectors by Williams *et al.* (1978) and Baker (1987). In the North, Emuruangogolak, Silali, Korosi and Ol Kokwe (Fig. 1) have erupted large volumes of basalts characterised by sparse pyroclastic activity (White *et al.,* 2012). In the southern Kenya Rift, basaltic eruptions have been typically minor but have occurred in the Ndabidi, Tandamara and Elementeita lava fields adjacent to the Olkaria, Suswa and Eburru calderas (Fig. 1; White *et al.,* 2012). Contemporary volcanism has also occurred to the East of the Rift, with Mt. Kenya, Mt. Meru and Mt. Kilimanjaro having erupted basalts alongside more differentiated nephelenite and phonolite compositions (Baker, 1987).

1.2 Strombolian activity in the EARS

Scoria (or cinder) cones are one of the most common volcanic landforms on Earth. They are characterised by Strombolian explosions that eject predominantly basaltic lapilli and ash tens to hundreds of meters into the air (Vespermann and Schminke, 2000; Fodor and Brož, 2015). Scoria cones are often described as parasitic, having formed due to eruptions along fissures on the flanks of a volcano rather than from the main vent. Hundreds of such cones form volcanic fields, which may be active over millions of years (Valentine and Connor, 2015) with average eruption recurrence intervals of hundreds to thousands of years (Ort *et al.,* 2008). Scoria cones are typically monogenetic*, i.e.* formed by a single episode of volcanism usually lasting days to weeks, although the more complex polygenetic character of some cones is now being recognised (*e.g*., Poppe et al., 2016). The eruption styles and landforms within volcanic fields are often variable: if magma interacts with water, explosive (phreatomagmatic) activity may form maar crater lakes and tuff cones, whereas if low-viscosity magma is erupted as a fire fountain, spatter cones of welded, ropey lava fragments may develop.

In equatorial East Africa, small basaltic cones occur along the flanks of both Mt. Meru and Mt. Kilimanjaro. Those on Mt. Meru are dated to 1.71 +/- 0.06 Ma (Wilkinson *et al.,* 1986), whereas those on Mt. Kilimanjaro are more recent and dated to 200-150 ka (Nonnotte *et al.,* 2008, 2011). Roughly 100 km to the east of the Kenya Rift, hundreds of basaltic scoria cones form the Hurri, Nyambeni and Chyulu Hills volcanic fields. Chyulu, the youngest and most southerly of these, hosts a minimum of 250 cones (as estimated from satellite imagery). Activity here is thought to have commenced around 1.4 Ma, and the young Shaitani and Chainu cones (Fig. 1) erupted as recently as the mid-19th century CE (Saggerson, 1963; Goles, 1975; Haug and Strecker, 1995; Späth *et al.,* 2000; 2001). Detailed studies (Haug and Strecker, 1995; Späth *et al.,* 2000; 2001) have resolved long-term trends in the volcanic history of the Chyulu Hills, but focused on dating effusive rather than explosive eruptions. This study provides the first detailed reconstruction of scoria-cone eruptions from volcanic fields on the shoulders of the Kenya-Tanzania Rift, including the Chyulu Hills.

1.3 Scoria cone eruptions recorded in lake sediments

Reconstruction of scoria-cone eruption histories is challenged by their association with lava flows and spatially-restricted scoria deposits, meaning that the imprint of past scoria-cone eruptions may be unrecognisable. However, these eruptions are capable of generating high eruption columns and extensive tephra fallout (*e.g.* Pioli *et al.,* 2008; Kawabata *et al.,* 2015; Jordan *et al.,* 2016). Scoria is particularly unstable and weathers readily, especially in tropical climates. Long inter-eruptive periods may therefore be associated with complex stratigraphic relationships, and deposits from older centres may be almost entirely denuded while new cones are developing (Németh *et al.,* 2012, 2014). The extent of scoria weathering and shape of the (remnant) cone may provide relative age control but, with datable minerals and charcoal often lacking, determining the absolute age of past eruptions can be difficult (Jaimes-Viera *et al.,* 2018; Nieto-Torres *et al.,* 2019).

Sedimentation in many lakes is continuous and uniform over long periods, providing a better-resolved and potentially more complete archive of regional volcanic history. Tephra layers preserved in lake sequences can often be dated using age-depth models built from ^{14}C dating of organic components – giving an indication of past eruption timing. Where comparative geochemical data is available for nearby volcanoes, and they erupt distinct magma compositions, the geochemistry of the glass shards composing the tephra can be used to identify its source. Tephra sequences in lake sediments have been widely used to constrain volcanic histories, typically from voluminous volcanic eruptions (*e.g.,* Lane *et al.,* 2017). However, several studies have also used lake sediment tephrostratigraphy to unravel the complex history of basaltic cones (*e.g.,* Green *et al.,* 2014; Hopkins *et al.,* 2015; 2017; Németh *et al.,* 2008). Studies on East African lake sequences (Martin-Jones *et al.,* 2017a; b; McNamara *et al.,* 2018; Lane *et al.,* 2018) are beginning to shed light on EARS volcanism, revealing the frequency of past, sometimes undocumented, eruptions. When these records can be linked with their on-land equivalents, they can also give an indication of eruption size.

In this study we present an initial tephrostratigraphic record of scoria-cone eruptions from volcanic fields in southern Kenya and northern Tanzania, derived from a ~250-ky sediment sequence from Lake Chala, a deep crater lake bridging the Kenya-Tanzania border on the south-eastern flank of Mt. Kilimanjaro. Lake Chala is relatively unique in having permanently stratified and anoxic bottom waters (Buckles *et al*., 2014), providing excellent preservation conditions for even very fine tephra layers from relatively modest and/or distant eruptions.

1.4 Lake Chala

Lake Chala (3.3° S; 37.7° E) is situated in a steep-sided volcanic crater basin formed after a monogenetic parasitic eruption associated with Mt. Kilimanjaro's most recent phase of volcanic activity. Based on the basal age of 25 ka for the upper, ^{14}C-dated, 21.65 metres of profundal sediments (Blaauw *et al*., 2011) and an extrapolated age model for the last 140 kyrs (Moernaut *et al.* 2010), Verschuren *et al*. (2013) estimated the age of the complete ~210-metre sediment infill in Lake Chala at >250,000 years. The lake is 94 m deep with a surface area of 4.2 km^2, and receives water only from direct rainfall, runoff from its steep crater walls and subsurface inflow originating from the percolation of rainfall onto the forest zone on Mt. Kilimanjaro (Verschuren *et al*., 2009). Its lower water column is permanently stratified, both today (Buckles *et al*. 2014; Wolff *et al*., 2014) and over at least the last 25,000 years (Verschuren et al. 2009). Consequently, Lake Chala accumulates undisturbed and near-continuously laminated diatomaceous organic sediments, interrupted only by turbidites and tephras (Verschuren *et al.,* 2013).

With the aim of reconstructing the palaeoclimate and landscape history of equatorial East Africa, two sediment sequences have been extracted from Lake Chala by the CHALLACEA and DeepCHALLA projects. The 21.65-m long composite CHALLACEA sequence was constructed from four overlapping piston cores collected in 2003 and 2005, and provided insights into climate dynamics spanning the last 25 kyr (*e.g*., Verschuren *et al.,* 2009; Barker *et al.,* 2011; Sinninghe Damsté *et al*., 2011). In November 2016, as part of the International Continental Scientific Drilling Program, the DeepCHALLA project (Verschuren *et al.,* 2013) retrieved a 215-m long sediment sequence, nearly reaching the crater floor. This study utilises both the CHALLACEA and DeepCHALLA sequences to explore its record of basaltic scoria-cone volcanism in the Mt. Kilimanjaro area.

Figure 1

2. Methods

2.1 Locating and analysing tephras

We identified and recorded basaltic tephra layers by visual inspection throughout the ~250-kyrs DeepCHALLA sequence, and documented their morphological features and crystal content under high-power microscopy. No visible tephra layers were detected in the CHALLACEA record, therefore this sequence was analysed for the presence of crypto-tephra using a method adapted from Blockley et al. (2005) and guided by peaks in XRF data (Kristen, 2007) indicating high concentrations of glass shards. Contiguous 1-cm samples were collected from the 10-cm sediment interval surrounding an XRF peak, dried at 95 °C, wet-sieved to >25 µm and then density-separated using a sodium polytungstate solution of >1.95 g/cm^3 to remove organic material. Extracted residues were counted under transmitted light microscopy and counts plotted against core stratigraphy to determine tephra isochrons (*i.e.,* the depth of peak shard density), from which shards were then sampled for geochemical analysis. For this purpose, both macro- and microscopic tephras were re-extracted from the sediment cores and sieved. Glass shards were mounted in epoxy resin stubs, which were then ground and polished to expose the glass for analysis.

Each tephra layer was assigned either a CHALLACEA (CH-) or DeepCHALLA (DCH-) code referring to the depth (in metres) of its basal contact according to the composite depth scale of both sequences, which corrects for core gaps and drilling-related artefacts but not for event deposits such as turbidites and tephra layers. Indicative ages (rounded to the nearest 0.1 ky for the CHALLACEA tephras and 1 ky for the DeepCHALLA tephras) were assigned to each tephra using the CHALLACEA ^{14}C-based chronology for the last 25 kyrs (CH-3.68 and CH-13.22; Blaauw *et al.,* 2011); links between Lake Chala seismic stratigraphy and known near-global climate events back to 140 ka (DCH-57.60, DCH-58.03, DCH-58.41, DCH-69.24, DCH-75.53, DCH-111.72 ; Moernaut *et al*., 2010); and extrapolation of the average sedimentation rate over this 140-ky interval (0.80 m/ky) to the base of the DeepCHALLA sequence (DCH-228.60; this study). At this time, the associated 95% age uncertainties are estimated to be ±0.1 ky (2.4%) for CH-3.68 and ±0.45 ky (2.7%) for CH-13.22 (Blaauw *et al*., 2011); ±2 ky (1.6-3%) for the six DeepCHALLA tephras <140 ka (Moernaut et al., 2010); and ±10 ky (4%) for DCH-228.60.

2.2. Tephra geochemical analyses

Individual glass shards from within all nine basaltic tephra layers, except CH-13.22, were analysed using a wavelength-dispersive Cameca SX-100 electron microprobe (WDS-EPMA) at the Department of Earth Sciences, University of Cambridge. CH-13.22 was analysed using a Jeol 8600 WDS-EPMA at the Research Laboratory for Archaeology and the History of Art, University of Oxford. Operating conditions were identical for both instruments, using a 10-μm diameter defocussed beam, a 15-kV accelerating voltage and 6-nA beam current. Sodium was collected for 10 s, Cl and P for 60 s and all other elements for 30 s. The instruments were calibrated against a series of mineral standards, and results were quantified using the PAP absorption correction method. Assays of the MPI-DING standards KL2-G (basalt) and St-Hs6/80-G (andesite) (Jochum *et al.,* 2006) and an in-house Lipari obsidian (peralkaline rhyolite) were used to monitor accuracy across the two instruments. All major element data presented in the text, tables and figures are normalised to 100% to account for variable secondary hydration of glasses. For raw data, see the Supplementary Material.

Trace element concentrations in individual glass shards were determined using a Thermo Scientific iCapQ coupled to a Teledyne G2 Eximer laser in the iCRAG laboratory at Trinity College Dublin. Depending on available sample areas, analyses used 20 μm^2, 30 μm^2 or 40 μm^2 laser spots. The laser was fired at a repetition rate of 5 Hz, with a count time of 40 seconds on both sample and gas blank. Concentrations were calculated via calibration against NIST612 and using ^{29}Si as the internal standard (concentrations determined via EPMA). Data reduction was performed in Iolite3.4, followed by a secondary correction using Ca as advocated in Tomlinson *et al.* (2010). To monitor instrument precision and accuracy, the MPI-DING reference materials GOR132-G (komatiite), St-Hs6/80-G (dacite) and ATHO-G (rhyolite) were analysed during each analytical run; see Supplementary Material for details.

2.3. Linking tephras to possible source regions

This study presents new glass data for nine tephra layers in Lake Chala sediments alongside published compositions of Kenya-Tanzania Rift volcanoes in order to identify their potential source volcanoes. When collating the reference dataset, we focussed on compositions of eruptions within the <250-ky time frame of the DeepCHALLA record. However, published compositional and chronological data from many EARS volcanoes are limited. Further, available compositions are frequently whole-rock data, which contain variable amounts of phenocrysts and hence preclude direct comparison of element concentrations (e.g. Smith *et al.,* 2005; Hopkins *et al.,* 2017; Pearce *et al.,* 2019). We therefore use a total alkali silica (TAS) plot (Le Bas *et al.,* 1986) to draw broad comparisons between eruptive compositions, and ratios of incompatible elements in glass or whole-rock samples to differentiate between eruption centres. Incompatible elements (e.g., Zr, Nb, Ba, La, and Pr) increase in abundance with magmatic differentiation, yet their ratios typically remain unchanged and can therefore be used as the chemical signature of an individual volcano. MacDonald (1987), Scott and Skilling (1999) and White *et al.* (2012) used Nb/Zr trends to discriminate among Kenyan Rift volcanoes, which are however more differentiated than the basaltic tephras in this study.

Results

3.1 Lake Chala tephrostratigraphy

This study focuses on nine basaltic tephras in the CHALLACEA and DeepCHALLA sequences (Table 1), which provide rare examples of far-travelled tephra from scoria-cone eruptions recorded in a lake-sediment archive. Seven of these tephras are macroscopically visible horizons in the DeepCHALLA record, containing light- to dark-brown scoriaceous, bubble-wall and ropey (>1000 μm in length) shard morphologies (Fig. 2) indicative of fragmentation through Strombolian-style eruption. Olivine and clinopyroxene crystals frequently occur both as phenocrysts and free crystals (Fig. 2). The glass shards are predominantly of alkaline basaltic composition, however one tephra at the base of the sequence contains foiditic (low SiO_2) glass (Fig. 3).

Cryptotephra investigation of the <25-ky sediments in the CHALLACEA sequence reveals regional volcanic activity into the Holocene. Background counts of glass shards are low, indicating that peaks in shard counts represent primary tephra deposition with little contamination from volcanic deposits forming the inner the crater walls. Two cryptotephra horizons (a modest peak of 100 shards/g dry sediment at 13.22 m depth and a more pronounced peak of 2230 shards/g dry sediment at 3.68 m depth) contain brown glass shards of alkaline basaltic composition (Fig. 3) similar to those in the DeepCHALLA sediments, and are therefore included in this study. For simplicity, these alkaline basaltic and foiditic tephras are hereafter referred to as mafic tephras.

Indicative ages for the nine mafic eruptions recorded in Lake Chala sediments are given in Table 1. The oldest tephra, found at the base of the DeepCHALLA sequence is dated to ~248 ka. All other investigated tephras were deposited during the last ~134 kyrs, with DCH-57.60, DCH-58.03 and DCH-58.41 deposited over a relatively short period between ~66 and ~65 kyrs. The youngest eruptions, recorded as cryptotephras in the CHALLACEA sequence, are dated to ~16.8 and ~4.2 ka.

Table 1

Figure 2

3.3 Composition of the mafic tephras in Lake Chala

Single-shard major and minor element concentrations are summarized in Table 2 and Figs. 3-5. Glass compositions and incompatible-element ratios permit discrimination between the individual tephras, as described below.

3.3.1 DeepCHALLA mafic tephras

The oldest of the mafic tephra layers in Lake Chala sediments (DCH-228.60; ~248 ka) occurs only 0.55 m above the base of the DeepCHALLA drill core. Glass shards within DCH-228.60 are foiditic and enriched in alkalis and the incompatible elements Zr, Nb, Ba, La, Pr and Nd; and depleted in MgO and TiO_2 relative to the other mafic tephras (Fig. 3).

Tephra DCH-228.60 as well as DCH-111.72 (~134 ka) and DCH-75.53 (~87 ka) show wide intra-eruptive variation in CaO content, distinguishing them from the more tightly constrained CaO concentrations in the six other tephras. Trends of Ba/La in DCH-111.72 and DCH-75.53 glass shards are distinct from one another and from those in the other mafic tephras. Glass shards in DCH-111.72 can be readily distinguished from DCH-75.53, because the latter are enriched in TiO2, MgO, FeO* and CaO; and depleted in SiO_2, Al_2O_3, the alkalis and Ba (Table 2, Figs. 4-5).

The four younger macroscopic mafic tephras derive from eruptions dated to between ~79 and ~65 kyrs, and occupy a similar area in the incompatible-element plots. Tephra DCH-69.24 (~79 ka) contains higher MgO and lower Al_2O_3 concentrations than DCH-58.41, DCH-58.03 and DCH-57.60 (~66-65 ka; Fig. 4). The latter three have similar major-element compositions, except that DCH-58.41 glass is enriched in MgO and depleted in Al_2O_3 relative to DCH-58.03; and that DCH-57.60 glass contains lower concentrations of incompatible trace elements (i.e. Zr, Nb, Ba, La, Pr) than all other tephras analysed.

3.3.2 CHALLACEA mafic cryptotephras

Brown glass shards in the CHALLACEA cryptotephras have major-element compositions that are most similar to the four youngest (~79–65 ky) visible tephras in the DeepCHALLA sequence (Figs. 3-4). The two cryptotephras cannot be distinguished from one another, as their composition is wide-ranging, each encompassing the entire range of MgO concentrations observed in the ~79–65 ky DeepCHALLA tephras. The cryptotephras do, however, contain slightly higher CaO and lower Al_2O_3 than the two youngest DeepCHALLA mafic tephras (Fig. 4).

<u>*Table 2*</u>

<u>*Figure 3*</u>

Figure 4

Figure 5

4. Discussion

4.1 Multi-criteria correlations

4.1.1. Major-, minor- and trace-element compositions

The mafic tephras in Lake Chala are more alkaline than basalts erupted from the Kenya Rift volcanoes (Fig. 3), and more closely resemble basalts erupted from the off-Rift volcanic centres of Mt. Kilimanjaro and the Chyulu Hills. The seven mafic DeepCHALLA tephras for which we have trace-element data show distinct linear arrays in plots of Ba/La, Pr/La and Zr/Nb (Fig. 5). The four younger tephras (DCH-69.24, DCH-58.41, DCH-58.03 and DCH-57.60) plot tightly along the same fractionation trends, whereas the three oldest tephras (DCH-228.60, DCH-111.72 and DCH-75.53) display incompatible-element trends that are distinct both from each other and from those younger tephras (Fig. 5).

Incompatible-element ratios of all mafic Chala tephras are broadly consistent with those of bulk alkaline lavas from the Chyulu Hills (Späth *et al.,* 2001) and Mt. Kilimanjaro's parasitic cones (Nonnotte *et al.,* 2011), which also plot within relatively well-defined values, particularly for Pr/La. Specifically, in plots of Pr/La and Zr/Nb, the four youngest mafic DeepCHALLA tephras track the same linear path as the Chyulu lavas, indicating that this is their likely source. Also tephra DCH-75.53 shows broadly similar incompatible-element ratios as the Chyulu lavas in terms of Pr/La and Zr/Nb, but is distinct in terms of Ba/La. However, since the latter ratio is less tightly constrained for Chyulu lavas, we tentatively suggest the Chyulu Hills is the most likely source for DCH-75.53. Without trace-element data we are unable to directly relate the <25-ky mafic cryptotephras to Chyulu or Mt. Kilimanjaro volcanism, notwithstanding their similarity in major-element composition to the ~79-65 ka tephras.

In contrast, the foiditic composition of tephra DCH-228.60 is more similar to the high alkalinity of parasitic volcanic activity on Mt. Kilimanjaro (Fig. 3). Both DCH-228.60 and DCH-111.72 follow a Pr/La trend similar to known Mt. Kilimanjaro tephras (Fig. 5) and we thus tentatively relate these two older mafic tephras to the later phase of Mt. Kilimanjaro volcanism as recognised by Nonnotte *et al.* (2011).

The compositional distinctions described above are subtle and it is therefore difficult, based on geochemistry alone, to confidently assign individual tephra layers to Mt. Kilimanjaro or the Chyulu Hills. Trends in published incompatible-element ratios for the Mt. Kilimanjaro and Chyulu lavas are not as tightly constrained as those in our glass data, and it is possible that only Pr and La, ratios of which are consistent between whole-rock samples and glass, behave as truly incompatible elements. The magmatic evolution of these two volcanic fields is likely complex, as both are fed by small magma batches derived from variable degrees of partial melting and crystal fractionation. The glass compositions of DCH-69.24, DCH-58.41, DCH-58.03 and DCH-57.60 follow crystallisation paths characteristic for olivine and clinopyroxene (Fig. 5). However, fluctuating concentrations of incompatible trace elements between them suggest a more complex magma evolution, possibly involving multiple influxes of fresh magma.

Haug and Strecker (1995) and Class *et al.* (1994) report both temporal and spatial variation in the geochemistry of lavas from the Chyulu Hills, with those erupted from cones in the south of the volcanic field enriched in SiO_2 compared to older northern lavas. Späth *et al.* (2000) attribute this change to the degree of partial melting increasing towards the South. Such differences in melting can create heterogeneous magma compositions across a single volcanic field, challenging comparisons using incompatible element ratios. Also, our understanding of compositional variation in magmas from the Chyulu volcanic fields is based only on studies of lava flows, which were erupted under different conditions, and likely at different times, to the tephras generated by explosive eruptions we observe in Lake Chala - further complicating direct comparisons.

4.1.2. Constraints from known eruption histories

Based on the compositional similarities discussed above, the two CHALLACEA cryptotephras and five youngest DeepCHALLA tephras (DCH-75.53, DCH-69.24, DCH-58.41, DCH-58.03 and DCH-57.60) are attributed to previously undefined eruptions of the Chyulu Hills, whilst DCH-228.60 and DCH-111.72 are tentatively correlated to Mt. Kilimanjaro. Further support for these proposed attributions is found in the known eruption history of these volcanic fields.

The Chyulu Hills is unique in the EARS for its prevalent Holocene volcanism (Saggerson, 1963; Haug and Strecker, 1995; Späth *et al.,* 2000; 2001). Lavas decrease in age from the northwest (~1.4 Ma) towards the southeast, where a lava flow East of Mzima Springs (Fig.

1b) overlies lake sediments radiocarbon-dated to ~26 ka (Späth *et al.,* 2000). Omenge and Okele (1992) provide oral accounts of <100-year-old flows from the Shaitani and Chainu cones in the South (Fig. 1). The Chyulu Hills is therefore younger than the most recent parasitic activity along the southeast flank of Mt. Kilimanjaro, which is dated to ~200-150 ka (Nonnotte *et al.,* 2008). Concordant with this older age, the Mt. Kilimanjaro scoria cones are typically more denuded and more densely vegetated than the Chyulu cones. The age of the two oldest (~248 ka and ~134 ka) mafic DeepCHALLA tephras is thus in line with the known timing of the final phases of volcanism on Mt. Kilimanjaro; and the prevalence of younger volcanic activity in the Chyulu Hills support our geochemical correlation of the two <25-ky CHALLACEA cryptotephras (4.2 and 16.8 ka) and five <100-ky DeepCHALLA tephras (between ~65 and ~87 ka) to that volcanic field. It should be noted, however, that the known eruption histories of Mt. Kilimanjaro and Chyulu are based on K/Ar dating of lavas collected from select areas of these volcanic fields, and hence may not capture all phases of their activity. Moreover, a complete cryptotephra scan of the long DeepCHALLA sediment record would likely document additional Chyulu Hills and Mt. Kilimanjaro eruptions.

4.1.3. Indications of source proximity

Mt. Kilimanjaro and the Chyulu Hills, the volcanic centres closest to Lake Chala that erupt basalts, are located respectively <1-30 km to the west, and 60-120 km to the northeast (Fig. 1). Tephra deposits typically become thinner and finer-grained with increasing distance from their source. Consistent with our source attributions, DCH-228.60 and DCH-111.72 contain broadly coarser (~300 µm) free crystals than the seven younger tephras (<100 µm; Table 1). Assuming modern wind patterns over the region, dispersal of tephra from the Chyulu Hills towards Lake Chala would vary seasonally, being promoted from November to April by northeasterly winds, and hampered from May to October by southeasterly winds (Wolff *et al.,* 2014).

4.2 Scoria-cone eruption records from lakes: potential and challenges

This study highlights the exceptional preservation conditions offered by lake systems such as Lake Chala, and their value in documenting eruptions otherwise unrecognised in the geological record. Tying the tephras incorporated in such lake records to their source is mainly challenged by the scarcity of published glass data characterising individual EARS volcanoes; this problem is amplified for intermittently active volcanic fields generating localised and rapidly-weathered basaltic scoria deposits. This study uses incompatible-element ratios to compare glass from mafic Chala tephras with published whole-rock analyses of lavas allowing their correlation to the Chyulu Hills and Mt. Kilimanjaro volcanic fields. Our geochemical correlations remain tentative however, as they are substantiated only by examining the Lake Chala tephrostratigraphy against existing, but skeletal, stratigraphic and geochronological outcrop data.

Further, whereas geochemical and chronological constraints allowed us to trace the mafic Chala tephras to two volcanic fields, correlating them to individual scoria cones is more challenging. As historical (<100 years) eruptions have been documented from the southerly Shaitani and Chainu cones in the Chyulu Hills, these, or cones nearby, are a likely source of the most recent (>4.2 ky) mafic cryptotephra recorded in Lake Chala. Späth et al. (2001) report that many of the Chyulu Hills cones, particularly from the southern sector, cannot be distinguished from one another based on their petrographic and geochemical characteristics. These difficulties call for more detailed study of the Chyulu Hills and Mt. Kilimanjaro volcanic fields, focussing not only on the lava flows but also past pyroclastic activity. Such compositional and chronological analysis should target the full temporal and spatial extent of these volcanic fields, allowing a detailed understanding of their eruptive history and magma genesis. Long sediment sequences, such as that of Lake Chala, have great potential to feed into our understanding of complex monogenetic volcanic fields, yet this potential can only be fully realised in the presence of detailed comparative eruption data from on-land records.

5. Conclusions

Mafic tephras preserved in Lake Chala sediments provide a new record of volcanic activity in the Chyulu Hills and Mt. Kilimanjaro volcanic fields spanning ~250,000 years. Excellent preservation conditions reveal tephra deposits from distant, and previously undocumented, scoria-cone eruptions. We tentatively attribute the two oldest mafic Chala tephras (dated to ~248 and ~134 ka) to Mt. Kilimanjaro, and seven younger tephras (dated to between ~87 and 4.2 kyrs) to volcanism in the Chyulu Hills. We show that pyroclastic activity has occurred in the Chyulu Hills over at least the last ~87 kyrs, and the ash deposited within the late-Holocene section of the Chala sequence supports the documented evidence of more recent volcanism. Pyroclastic activity will likely continue to be a common feature of future volcanism in the Chyulu Hills, however detailed research into the volcanological hazard and associated socio-cultural implications is needed to evaluate the extent of any risks to the local population.

Acknowledgements

This research was funded jointly by a UK Natural Environment Research Council standard grant (NE/P011969/1) and the International Continental Scientific Drilling Program through the DeepCHALLA project (https://www.icdp-online.org/projects/world/africa/lake-challa-kenya-tanzania/). The authors thank the DeepCHALLA science team and Karen Fontijn for their contributions and discussion of ideas. Cryptotephra analyses were carried out in the Cambridge Tephra Laboratory, within the Department of Geography Science Laboratories at the University of Cambridge. Alma Piermattei and Friederike Murach-Ward assisted with cryptotephra analysis, which were begun as part of an Early Career Fellowship from the Leverhulme Trust to CSL. Iris Buisman and Victoria Smith kindly supported EPMA analysis. We thank Karoly Németh and an anonymous reviewer for their suggestions, which greatly improved an earlier draft of this paper.

References

Baker, B.H., 1987. Outline of the petrology of the Kenya rift alkaline province. *Geological Society, London, Special Publications*, *30*(1), pp.293-311.

Barker, P.A., Hurrell, E.R., Leng, M.J. *et al.* 2011. Seasonality in equatorial climate over the past 25 ky revealed by oxygen isotope records from Mount Kilimanjaro. *Geology*, *39*(12), pp.1111-1114.

Blaauw, M., van Geel, B., Kristen, I. *et al.* 2011. High-resolution 14C dating of a 25,000-year lake-sediment record from equatorial East Africa. *Quaternary Science Reviews*, *30*(21-22), pp.3043-3059.

Blegen, N., Brown, F.H., Jicha, B.R. *et al.* 2016. The Menengai Tuff: A 36 ka widespread tephra and its chronological relevance to Late Pleistocene human evolution in East Africa. *Quaternary Science Reviews*, *152*, pp.152-168.

Blegen, N., Jicha, B.R. and McBrearty, S., 2018. A new tephrochronology for early diverse stone tool technologies and long-distance raw material transport in the Middle to Late Pleistocene Kapthurin Formation, East Africa. *Journal of human evolution*, *121*, pp.75-103.

Blockley, S.P.E., Pyne-O'Donnell, S.D.F., Lowe, J.J. *et al.* 2005. A new and less destructive laboratory procedure for the physical separation of distal glass tephra shards from sediments. *Quaternary Science Reviews*, *24*(16-17), pp.1952-1960.

Brown, F.H., Nash, B.P., Fernandez, D.P. *et al.* 2013. Geochemical composition of source obsidians from Kenya. *Journal of Archaeological Science*, *40*(8), pp.3233-3251.

Buckles, L.K., Weijers, J.W., Verschuren, D. *et al.* 2014. Sources of core and intact branched tetraether membrane lipids in the lacustrine environment: Anatomy of Lake Challa and its catchment, equatorial East Africa. *Geochimica et Cosmochimica Acta*, *140*, pp.106-126.

Campisano, C.J., Cohen, A.S., Arrowsmith, J.R. *et al.* 2017. The Hominin Sites and Paleolakes Drilling Project: High-resolution paleoclimate records from the East African Rift System and their implications for understanding the environmental context of hominin evolution. *PaleoAnthropology*.

Carr, M.J. and Gazel, E., 2017. Igpet software for modeling igneous processes: examples of application using the open educational version. *Mineralogy and Petrology*, *111*(2), pp.283-289.

Class, C., Altherr, R., Volker, F. *et al.* 1994. Geochemistry of Pliocene to Quaternary alkali basalts from the Huri Hills, northern Kenya. *Chemical Geology*, *113*(1-2), pp.1-22.

Feakins, S.J., Brown, F.H. and deMenocal, P.B., 2007. Plio-Pleistocene microtephra in DSDP site 231, Gulf of Aden. *Journal of African Earth Sciences*, *48*(5), pp.341-352.

Fodor, E. and Brož, P., 2015. Cinder Cone. In: H. Hargitai and Á. Kereszturi (Editors), Encyclopedia of Planetary Landforms. Springer New York, New York, NY, pp. 290-295.

Fontijn, K., Ernst, G.G., Elburg, M.A. *et al.* 2010. Holocene explosive eruptions in the Rungwe Volcanic Province, Tanzania. *Journal of Volcanology and Geothermal Research*, *196*(1-2), pp.91-110.

Fontijn, K., McNamara, K., Tadesse, A.Z. *et al.* 2018. Contrasting styles of post-caldera volcanism along the Main Ethiopian Rift: Implications for contemporary volcanic hazards. *Journal of Volcanology and Geothermal Research*, *356*, pp.90-113.

Global Volcanism Program, 2013. Volcanoes of the World, v.4.8.0, Venzke, E. (ed.). Smithsonian Institution. Downloaded 21st October 2018. https://doi.org/10.5478/si.GVP.VOTW4-2013

Goles, G.G., 1975. Basalts of unusual composition from the Chyulu Hills, Kenya. *Lithos*, *8*(1), pp.47-58.

Green, R.M., Bebbington, M.S., Cronin, S.J. *et al.* 2014. Automated statistical matching of multiple tephra records exemplified using five long maar sequences younger than 75 ka, Auckland, New Zealand. *Quaternary Research*, *82*(2), pp.405-419.

Haug, G.H. and Strecker, M.R., 1995. Volcano-tectonic evolution of the Chyulu Hills and implications for the regional stress field in Kenya. *Geology*, *23*(2), pp.165-168.

Hasenaka, T. and Carmichael, I.S., 1985. The cinder cones of Michoacán—Guanajuato, central Mexico: their age, volume and distribution, and magma discharge rate. *Journal of Volcanology and Geothermal Research*, *25*(1-2), pp.105-124.

Hay, R.L., 1989. Holocene carbonatite-nephelinite tephra deposits of Oldoinyo Lengai, Tanzania. *Journal of Volcanology and Geothermal Research*, *37*(1), pp.77-91.

Hopkins, J.L., Millet, M.A., Timm, C. *et al.* 2015. Tools and techniques for developing tephra stratigraphies in lake cores: a case study from the basaltic Auckland Volcanic Field, New Zealand. *Quaternary Science Reviews*, *123*, pp.58-75.

Irvine, T.N.J. and Baragar, W.R.A., 1971. A guide to the chemical classification of the common volcanic rocks. *Canadian journal of earth sciences*, *8*(5), pp.523-548.

Jaimes-Viera, M.C., Del Pozzo, A.M., Layer, P.W. *et al.* 2018. Timing the evolution of a monogenetic volcanic field: Sierra Chichinautzin, Central Mexico. *Journal of Volcanology and Geothermal Research*, *356*, pp.225-242.

Jochum, K.P., Stoll, B., Herwig, K. *et al.* 2006. MPI-DING reference glasses for in situ microanalysis: New reference values for element concentrations and isotope ratios. *Geochemistry, Geophysics, Geosystems*, *7*(2).

Jordan, S.C., Le Pennec, J.L., Gurioli, L. *et al.* 2016. Highly explosive eruption of the monogenetic 8.6 ka BP La Vache et Lassolas scoria cone complex (Chaîne des Puys, France). *Journal of Volcanology and Geothermal Research*, *313*, pp.15-28.

Kawabata, E., Cronin, S.J., Bebbington, M.S. *et al.* 2015. Identifying multiple eruption phases from a compound tephra blanket: an example of the AD1256 Al-Madinah eruption, Saudi Arabia. *Bulletin of Volcanology*, *77*(1), pp.6.

Kristen, I., 2010. *Investigations on rainfall variability during the late Quaternary based on geochemical analyses of lake sediments from tropical and subtropical southern Africa*. GeoForschungsZentrum Potsdam.

Lane, C.S., Lowe, D.J., Blockley, S.P.E. *et al.* 2017. Advancing tephrochronology as a global dating tool: applications in volcanology, archaeology, and palaeoclimatic research.

Lane, C.S., Martin-Jones, C.M. and Johnson, T.C., 2018. A cryptotephra record from the Lake Victoria sediment core record of Holocene palaeoenvironmental change. *The Holocene*, *28*(12), pp.1909-1917.

Le Bas, M. Le Maitre, R., Streckeisen, A., Zanettin, B., & IUGS Subcommission on the Systematics of Igneous Rocks, 1986. A chemical classification of volcanic rocks based on the total alkali-silica diagram. *Journal of Petrology*, *27*(3), pp.745-750.

Luhr, J. F., Simkin, T., & Cuasay, M., 1993. *Parícutin: the volcano born in a Mexican cornfield*. US Geoscience Press. pp.427.

Macdonald, R., 1987. Quaternary peralkaline silicic rocks and caldera volcanoes of Kenya. *Geological Society, London, Special Publications*, *30*(1), pp.313-333.

Macdonald, R., Davies, G.R., Upton, B.G.J. *et al.* 1995. Petrogenesis of Silali volcano, Gregory Rift, Kenya. *Journal of the Geological Society*, *152*(4), pp.703-720.

Marshall, A., Macdonald, R., Rogers, N.W. *et al.* 2009. Fractionation of peralkaline silicic magmas: The greater olkaria volcanic complex, Kenya Rift Valley. *Journal of Petrology*, *50*(2), pp.323-359.

McDOUGALL, I.A.N. and Brown, F.H., 2009. Timing of volcanism and evolution of the northern Kenya Rift. *Geological Magazine*, *146*(1), pp.34-47.

Martin-Jones, C.M., Lane, C.S., Pearce, N.J.G. *et al.* 2017. Glass compositions and tempo of post-17 ka eruptions from the Afar Triangle recorded in sediments from lakes Ashenge and Hayk, Ethiopia. *Quaternary Geochronology*, *37*, pp.15-31.

Martin-Jones, C.M., Lane, C.S., Pearce, N.J.G. *et al.* 2017. Recurrent explosive eruptions from a high-risk Main Ethiopian Rift volcano throughout the Holocene. *Geology*, *45*(12), pp.1127-1130.

McNamara, K., Cashman, K.V., Rust, A.C. *et al.* 2018. Using lake sediment cores to improve records of volcanism at Aluto volcano in the Main Ethiopian Rift. *Geochemistry, Geophysics, Geosystems*, *19*(9), pp.3164-3188.

Moernaut, J., Verschuren, D., Charlet, F. *et al.* 2010. The seismic-stratigraphic record of lake-level fluctuations in Lake Challa: Hydrological stability and change in equatorial East Africa over the last 140 kyr. *Earth and Planetary Science Letters*, *290*(1-2), pp.214-223.

Németh, K., Goth, K., Martin, U. *et al.* 2008. Reconstructing paleoenvironment, eruption mechanism and paleomorphology of the Pliocene Pula maar (Hungary). *Journal of Volcanology and Geothermal Research*, *177*(2), pp.441-456.

Németh, K., 2010. Monogenetic volcanic fields: Origin, sedimentary record, and relationship with polygenetic volcanism. In: E. Canon-Tapia and A. Szakacs (Editors), What Is a Volcano? Geological Society of America, Boulder, Colorado, vol. 470, pp. 43-66.

Németh, K., 2012. A nested polymagmatic and polycyclic tuff ring and scoria cone complex at Chaguido (Jeju Island), South Korea. *Geoscience Society of New Zealand Miscellaneous Publication 131A*, p.68.

Németh, K., Moufti, M.R., El-Masry, N. *et al.* 2014. Maars over cones: repeated volcanism in the same location along fissures in western Saudi Arabian volcanic fields. In *5th International Maar Conference. Universidad Nacional Autónoma de México, Centro de Geociencias, Juriquilla, Querétaro, México* (pp. 2-3).

Nieto-Torres, A. and Del Pozzo, A.L.M., 2019. Spatio-temporal hazard assessment of a monogenetic volcanic field, near México City. *Journal of Volcanology and Geothermal Research*, *371*, pp.46-58.

Nonnotte, P., Guillou, H., Le Gall, B. *et al.* 2008. New K–Ar age determinations of Kilimanjaro volcano in the North Tanzanian diverging rift, East Africa. *Journal of Volcanology and Geothermal Research*, *173*(1-2), pp.99-112.

Nonnotte, P., Benoit, M., Le Gall, B. *et al.* 2011. Petrology and geochemistry of alkaline lava series, Kilimanjaro, Tanzania: new constraints on petrogenetic processes. *Geol. Soc. Am. Spec. Pap*, *478*, pp.127-158.

Ort, M.H., Elson, M.D., Anderson, K.C. *et al.* 2008. Effects of scoria-cone eruptions upon nearby human communities. *Geological Society of America Bulletin*, *120*(3-4), pp.476-486.

Omenge, J.M. and Okele, R.E., 1992. *Geology of the Chyulu-Oloitokitok area. Kenya Mines and Geology Department, Nairobi, Geological Survey of Kenya* (No. 112).

Pioli, L., Erlund, E., Johnson, E. *et al.* 2008. Explosive dynamics of violent Strombolian eruptions: the eruption of Parícutin Volcano 1943–1952 (Mexico). *Earth and Planetary Science Letters*, *271*(1-4), pp.359-368.

Poppe, S., Smets, B., Fontijn, K. *et al.* 2016. Holocene phreatomagmatic eruptions alongside the densely populated northern shoreline of Lake Kivu, East African Rift: timing and hazard implications. *Bulletin of volcanology*, *78*(11), p.82.

Ren, M., Omenda, P.A., Anthony, E.Y. *et al.* 2006. Application of the QUILF thermobarometer to the peralkaline trachytes and pantellerites of the Eburru volcanic complex, East African Rift, Kenya. *Lithos*, *91*(1-4), pp.109-124.

Roberts, M. A. (2003). *Geochemical and volcanological evolution of the Mt. Meru region, northern Tanzania* (Doctoral dissertation, University of Cambridge). pp.120.

Rogers, N.W., Evans, P.J., Blake, S. *et al.* 2004. Rates and timescales of fractional crystallization from ^{238}U–^{230}Th–^{226}Ra disequilibria in trachyte lavas from Longonot volcano, Kenya. *Journal of Petrology*, *45*(9), pp.1747-1776.

Saggerson, E.P., 1963. Geology of the Simba-Kibwezi Area: Ministry of Commerce and Industry Geological Survey of Kenya, pp 53.

Scott, S.C. and Skilling, I.P., 1999. The role of tephrachronology in recognizing synchronous caldera-forming events at the Quaternary volcanoes Longonot and Suswa, south Kenya Rift. *Geological Society, London, Special Publications*, *161*(1), pp.47-67.

Damsté, J.S.S., Verschuren, D., Ossebaar, J. *et al.* 2011. A 25,000-year record of climate-induced changes in lowland vegetation of eastern equatorial Africa revealed by the stable carbon-isotopic composition of fossil plant leaf waxes. *Earth and Planetary Science Letters*, *302*(1-2), pp.236-246.

Smith, V.C., Shane, P. and Nairn, I.A., 2005. Trends in rhyolite geochemistry, mineralogy, and magma storage during the last 50 kyr at Okataina and Taupo volcanic centres, Taupo Volcanic Zone, New Zealand. *Journal of Volcanology and Geothermal Research*, *148*(3-4), pp.372-406.

Späth, A., Le Roex, A.P. and Opiyo-Akech, N., 2000. The petrology of the Chyulu Hills volcanic province, southern Kenya. *Journal of African Earth Sciences*, *31*(2), pp.337-358.

Späth, A., Le Roex, A.P. and Opiyo-Akech, N., 2001. Plume–lithosphere interaction and the origin of continental rift-related alkaline volcanism—the Chyulu Hills volcanic province, southern Kenya. *Journal of Petrology*, *42*(4), pp.765-787.

Tomlinson, E.L., Thordarson, T., Müller, W. *et al.* 2010. Microanalysis of tephra by LA-ICP-MS—strategies, advantages and limitations assessed using the Thorsmörk Ignimbrite (Southern Iceland). *Chemical Geology*, *279*(3-4), pp.73-89.

Tryon, C.A. and McBrearty, S., 2002. Tephrostratigraphy and the Acheulian to Middle Stone Age transition in the Kapthurin formation, Kenya. *Journal of Human Evolution*, *42*(1-2), pp.211-235.

Tryon, C.A. and McBrearty, S., 2006. Tephrostratigraphy of the Bedded Tuff Member (Kapthurin Formation, Kenya) and the nature of archaeological change in the later Middle Pleistocene. *Quaternary Research*, *65*(3), pp.492-507.

Tryon, C.A., Roach, N.T. and Logan, M.A.V., 2008. The Middle Stone Age of the northern Kenyan Rift: age and context of new archaeological sites from the Kapedo Tuffs. *Journal of Human Evolution*, *55*(4), pp.652-664.

Valentine, G.A. and Connor, C.B., 2015. Basaltic volcanic fields. In *The Encyclopedia of Volcanoes* (pp. 423-439). Academic Press.

Verschuren, D., Damsté, J.S.S., Moernaut, J. *et al.* 2009. Half-precessional dynamics of monsoon rainfall near the East African Equator. *Nature*, *462*(7273), p.637.

Verschuren, D., Olago, D.O., Rucina, S.M. *et al.* 2013. DeepCHALLA: Two glacial cycles of climate and ecosystem dynamics from equatorial East Africa. *Scientific Drilling*, *15*, pp.72-76.

Vespermann, D. and Schmincke, H.-U., 2000. Scoria cones and tuff rings. In: H. Sigurdsson, B.F. Houghton, S.R. McNutt, H. Rymer and J. Stix (Editors), Encyclopedia of Volcanoes. Academic Press, San Diego, pp. 683-694.

White, J.C., Espejel-García, V.V., Anthony, E.Y. *et al.* 2012. Open system evolution of peralkaline trachyte and phonolite from the Suswa volcano, Kenya rift. *Lithos*, *152*, pp.84-104.

Williams, L.A., 1978. Character of Quaternary volcanism in the Gregory rift valley. *Geological Society, London, Special Publications*, *6*(1), pp.55-69.

Williams, S.N., 1983. Plinian airfall deposits of basaltic composition. *Geology*, *11*(4), pp.211-214.

Wilkinson, P., Mitchell, J.G., Cattermole, P.J. *et al.* 1986. Volcanic chronology of the Men–Kilimanjaro region, Northern Tanzania. *Journal of the Geological Society*, *143*(4), pp.601-605.

Wolff, C., Kristen-Jenny, I., Schettler, G. *et al.* 2014. Modern seasonality in Lake Challa (Kenya/Tanzania) and its sedimentary documentation in recent lake sediments. *Limnology and Oceanography*, *59*(5), pp.1621-1636.

Table 1. *Identification code, location in the sediment sequence (core section and depth, at base of deposit), physical properties and age of the mafic DeepCHALLA tephras (DCH-) and CHALLACEA cryptotephras (CH-) analysed in this study. Minerals are abbreviated as cpx (clinopyroxene), ol (olivine) and fsp (feldspar). The listed ages are based on ^{14}C dating for the two CHALLACEA cryptotephras (Blaauw et al., 2011), and an extrapolated age model tied to seismic stratigraphy (Moernaut et al., 2010) for the seven DeepCHALLA tephras. Age uncertainties are 2.4-2.7% for CH tephras and 1.6-4% for DCH tephras; see text.*

Tephra ID	*Core section*	*Section depth*	*Composite depth (m)*	*Thickness (cm)*	*Glass size*	*Crystals*	*Crystal size (μm)*	*Age (ka)*
CH-3.68	2PII	45.4	3.68	-	<100	trace	<50	4.2
CH-13.22	3P-Va	104.6	13.22	-	<50	trace	<50	16.8
DCH-57.60	1B-18H-2	56.5	57.6	0.5	<1000	cpx, ol	<100	~65
DCH-58.03	1B-18H-2	99.5	58.03	0.5	<1000	cpx, ol	<100	~65
DCH-58.41	1B-18H-3	21.5	58.41	0.3	<1000	cpx, ol	<100	~66
DCH-69.24	1A-23H-2	23.3	69.24	0.3	<100	trace	<100	~79
DCH-75.53	1B-23H-3	51.8	75.53	0.3	<250	trace	<100	~87
DCH-111.72	1B-35H-1	34	111.72	0.5	<600	fsp, cpx	<300	~134
DCH-228.60	1E-45E-3	122.5	228.6	1	<1000	fsp, cpx	<250	~248

Table 2. *Average major-, minor- (wt.%) and trace-element (ppm) concentrations of the mafic DeepCHALLA and CHALLACEA tephras, with standard deviation added in italics and the number of shards analysed at the top of each data column. Major and minor elements are normalised to 100% analytical totals, ‘<bd’’ indicates concentrations below instrument detection limit. See Supplementary Information for raw data and analyses of reference materials.*

	Challacea				DeepCHALLA													
	CH-3.68		CH-13.22		DCH-57.60		DCH-58.03		DCH-58.41		DCH-69.24		DCH-75.53		DCH-111.72		DCH-228.60	
	n=5		*n=35*		*n=30*		*n=24*		*n=29*		*n=30*		*n=26*		*n=16*		*n=30*	
SiO_2	45.24	1.14	46.48	1.80	45.06	0.55	45.25	1.50	45.26	0.66	44.81	0.58	44.56	0.83	46.07	1.66	44.89	0.69
TiO_2	4.28	0.16	4.33	0.29	4.46	0.22	4.33	0.62	4.43	0.14	4.41	0.12	4.56	0.22	3.95	0.26	3.37	0.22
Al_2O_3	14.30	0.58	14.59	1.13	15.05	0.67	15.23	1.19	14.64	0.35	13.75	0.34	13.74	1.39	15.61	0.71	16.03	0.56
MgO	5.39	0.65	5.17	1.75	5.28	0.76	4.62	0.55	4.93	0.44	5.87	0.49	5.06	1.18	4.10	0.81	4.07	0.48
FeO^T	13.44	1.00	12.52	1.45	13.35	0.55	12.75	1.37	12.78	0.74	13.54	0.51	13.65	1.24	12.21	0.68	11.19	0.56
MnO	0.21	0.09	0.18	0.11	0.18	0.07	0.20	0.11	0.22	0.10	0.21	0.06	0.23	0.10	0.21	0.05	0.26	0.14
CaO	11.05	0.43	10.74	2.11	10.70	0.69	10.53	1.14	10.96	0.49	11.24	0.23	11.72	1.72	10.10	1.36	9.79	0.96
Na_2O	3.74	0.43	3.53	1.23	3.76	0.46	4.35	0.64	4.09	0.57	3.71	0.31	4.03	0.85	4.42	0.64	6.15	0.60
K_2O	1.55	0.14	1.70	0.65	1.48	0.13	1.79	0.27	1.80	0.17	1.68	0.13	1.61	0.26	2.33	0.28	2.91	0.29
P_2O_5	0.80	0.12	0.77	0.32	0.67	0.07	0.94	0.21	0.90	0.11	0.78	0.09	0.85	0.15	0.97	0.15	1.33	0.13
					n=20		*n=16*		*n=15*		*n=20*		*n=15*		*n=15*		*n=18*	
Rb					33.1	1.53	42.4	11.4	43.9	3.59	40.4	1.98	43.7	7.66	69.2	11.62	73.1	7.86
Sr					802	38.1	940	102	963	114	878	41.6	1020	138	1212	118	1530	149
Y					30.2	1.08	37.1	3.28	35.2	3.87	32.3	1.82	38.0	4.14	36.4	5.96	36.2	2.94
Zr					331	14.3	439	91.5	452	46.4	366	19.5	468	35.7	430	47.9	480	34.3
Nb					79.6	3.30	106	18.1	108	11.8	93.2	3.19	126	14.2	151	12.8	187	15.6
Cs					0.32	0.048	0.45	0.23	0.44	0.10	0.40	0.042	0.44	0.11	<lld	<lld	0.74	0.083
Ba					462	21.2	614	86.8	647	73.6	542	22.0	598	81.4	1020	95.7	1192	106
La					58.3	2.52	82.1	16.2	84.8	9.40	71.6	3.37	102	12.0	115	11.7	162	12.6
Ce					123	6.45	174	29.9	179	22.4	148	6.53	215	22.7	221	24.5	307	23.1
Pr					14.0	0.627	20.1	3.13	20.6	2.64	16.7	1.04	24.1	2.60	23.3	3.07	32.0	2.42
Nd					60.1	2.86	83.4	11.4	85.1	10.6	69.0	3.02	92.5	11.0	89.6	14.4	117	8.91
Sm					11.9	0.719	15.2	2.23	15.8	2.26	13.1	0.912	16.6	2.22	15.3	2.51	18.5	1.63

Eu		**3.53**	0.193	**4.59**	*0.495*	**4.48**	*0.561*	**3.77**	*0.207*	**4.73**	*0.563*	<bd	<bd	**5.10**	*0.408*
Dy		**7.11**	0.341	**9.52**	*1.03*	**8.61**	*1.42*	**7.48**	*0.520*	**8.94**	*1.32*	<bd	<bd	**8.24**	*0.805*
Er		**2.94**	0.165	**3.96**	*0.806*	**3.54**	*0.678*	**3.17**	*0.263*	**3.76**	*0.520*	<bd	<bd	**3.54**	*0.339*
Yb		**2.26**	0.180	**2.96**	*0.451*	**2.74**	*0.611*	**2.35**	*0.232*	**2.80**	*0.577*	<bd	<bd	**2.82**	*0.444*
Hf		**7.55**	0.421	**10.7**	*1.60*	**10.1**	*1.61*	**8.32**	*0.766*	**10.7**	*1.50*	**8.84**	*1.58*	**8.95**	*0.945*
Ta		**4.72**	0.214	**6.47**	*0.764*	**6.59**	*0.847*	**5.54**	*0.306*	**7.63**	*1.02*	**8.51**	*0.916*	**10.2**	*0.816*
Pb		**4.17**	0.583	**6.14**	*3.41*	**6.74**	*3.08*	**5.03**	*0.643*	**6.25**	*1.54*	**10.0**	*3.14*	**11.7**	*2.70*
Th		**6.52**	0.346	**9.68**	*2.54*	**9.62**	*1.64*	**8.00**	*0.642*	**11.2**	*1.52*	**14.7**	*2.42*	**19.2**	*1.70*
U		**1.65**	0.162	**2.71**	*1.22*	**2.62**	*0.491*	**1.98**	*0.169*	**2.93**	*0.424*	**3.46**	*0.441*	**4.83**	*0.551*

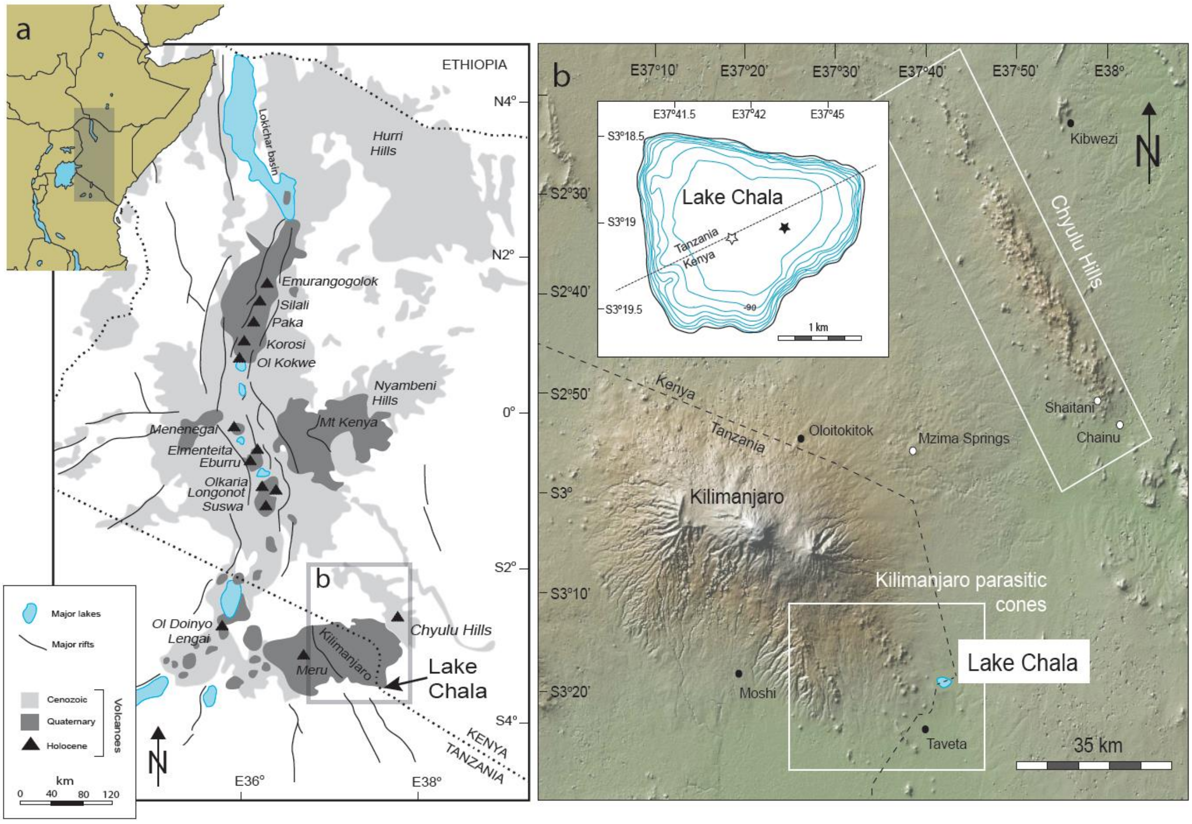

__Fig. 1__ Study area and geographical context. (a) Volcanic and tectonic features of the East African Rift System in Kenya and northern Tanzania (grey box in the inset map of East Africa shows location), with spatial extent of Cenozoic and Quaternary volcanism (light and dark grey shading) redrawn after Späth et al. (2001), and locations of Holocene volcanoes (triangles) extracted from the Global Volcanism Program (2013) online database. (b) Digital elevation model of the study area in southeastern Kenya and northeastern Tanzania (box in panel a) with location of Lake Chala relative to the Mt. Kilimanjaro and Chyulu Hills volcanic fields (white boxes). Major settlements and locations referred to in the text are indicated with black and white circles, respectively. The inset map shows the bathymetry of Lake Chala (in metres) with indication of the CHALLACEA (white star) and DeepCHALLA (black star) coring sites.

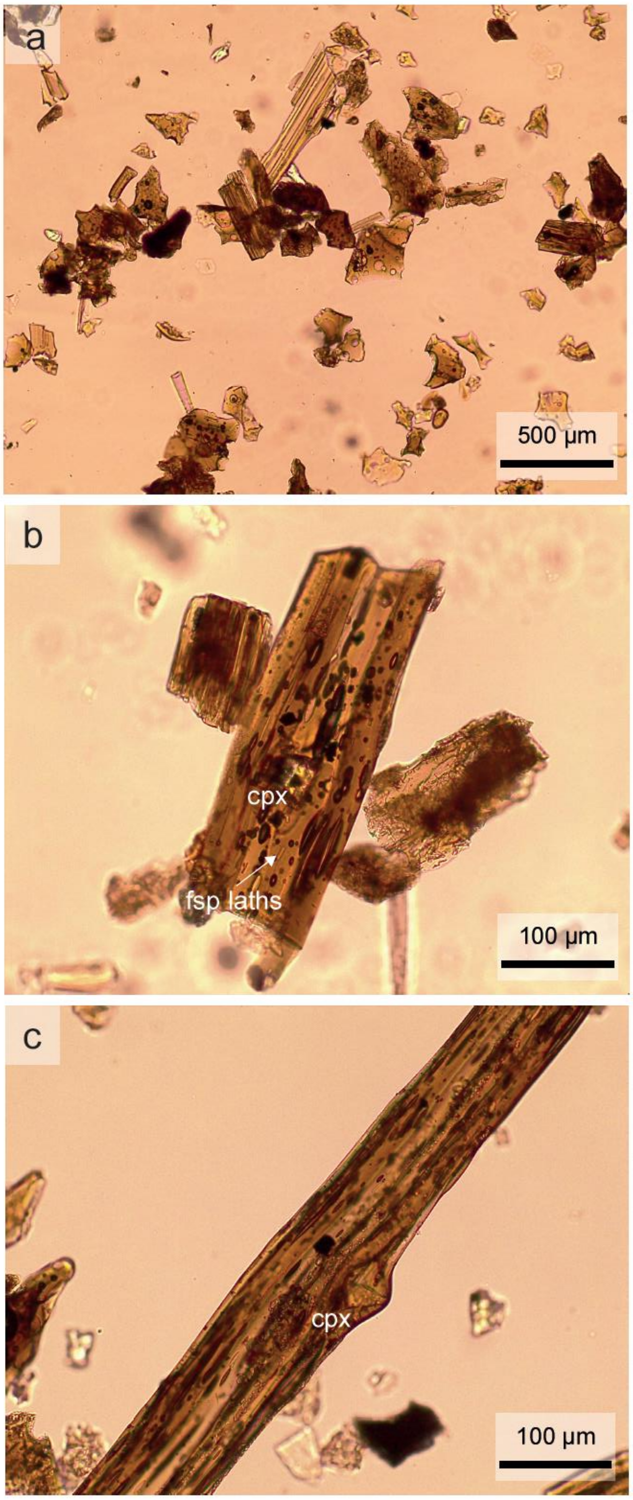

Fig. 2 *Distinctive mafic glass-shard morphologies in Lake Chala sediments. (a) typical mafic shard assemblage. (b-c) individual shards with clinopyroxene phenocrysts and minor feldspar laths.*

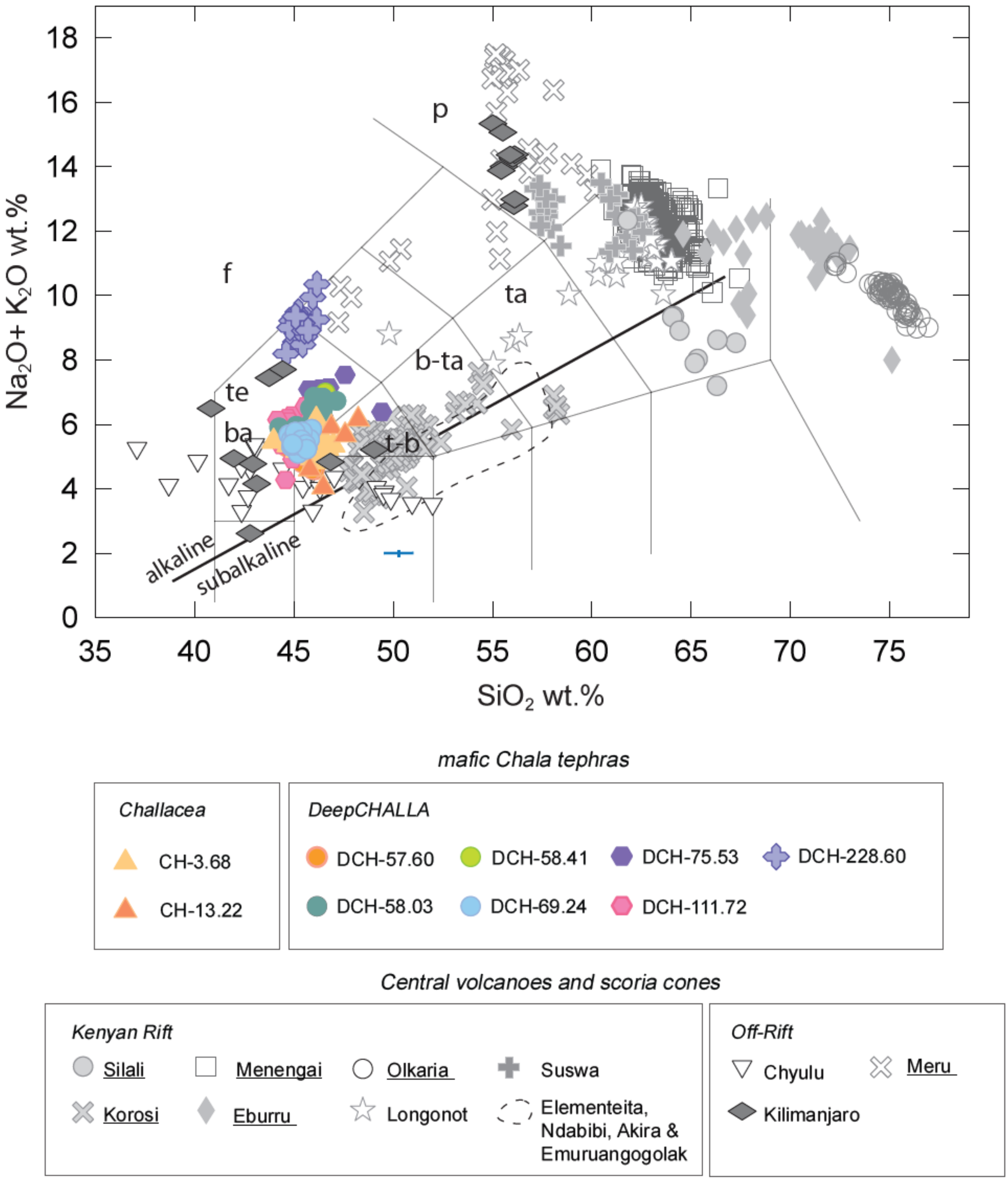

18
16
14
12
10
8
6
4
2
0
35
40
45
50
55
60
65
70
75
Na_2O+ K_2O wt.%
SiO_2 wt.%
p
f
ta
b-ta
te
ba
t-b
alkaline
subalkaline
mafic Chala tephras
Challacea
CH-3.68
CH-13.22
DeepCHALLA
DCH-57.60
DCH-58.41
DCH-75.53
DCH-228.60
DCH-58.03
DCH-69.24
DCH-111.72
Central volcanoes and scoria cones
Kenyan Rift
Silali
Menengai
Olkaria
Suswa
Korosi
Eburru
Longonot
Elementeita, Ndabibi, Akira & Emuruangogolak
Off-Rift
Chyulu
Meru
Kilimanjaro

Fig. 3 *Total alkali-silica (TAS) plot showing glass composition of the nine mafic Chala tephras analysed in this study. Error bars (blue cross, 2 sigma) are based on repeat analyses of the MPI-DING basalt standard KL2-G, averaged across all analytical runs. Compositional fields referred to in the text are foidite (f), tephrite (te), basanite (ba), trachybasalt (t-b), basaltic trachyandesite (b-ta), trachyandesite (ta) and phonolite (p) (Le Bas et al., 1986). Alkaline and subalkaline fields are according to Irvine and Barager (1971). Published compositions of tephra and lavas from Kenyan and Tanzanian volcanoes (and dated to the Late Pleistocene or Holocene; Fig. 1), are plotted for comparison. Volcanoes with glass data are underlined in the legend, other data are based on whole-rock analyses. Source publications as follows:* ***Elementeita, Ndabibi, Akira*** *and* ***Emuruangoglak*** *Rift basalts: compositional envelope from White et al. (2012);* ***Silali****: the ~130-120 ka Kapedo Tuffs, from Tryon et al. (2008);* ***Korosi:*** *the Bedded Tuff Member from Tryon and McBrearty (2002; 2006) and Blegen et al. (2018);* ***Menengai****: the ~36 ka tuff from Blegen et al. (2016);* ***Eburru****: analyses of lava, pyroclastics (Ren et al., 2006) and obsidians (Brown et al., 2013);* ***Olkaria****: obsidians from Marshall et al. (2009) and Brown et al. (2013);* ***Longonot****: pumice (Scott and Skilling, 1999) and lavas (Rogers et al., 2004);* ***Suswa****: lavas and tuffs (White et al., 2012);* ***Meru****: pumice (Fontijn and Lane, unpublished data), lavas and tuff (Roberts, 2003);* ***Kilimanjaro****: Nonnotte et al. (2011);* ***Chyulu****: Späth et al. (2001).*

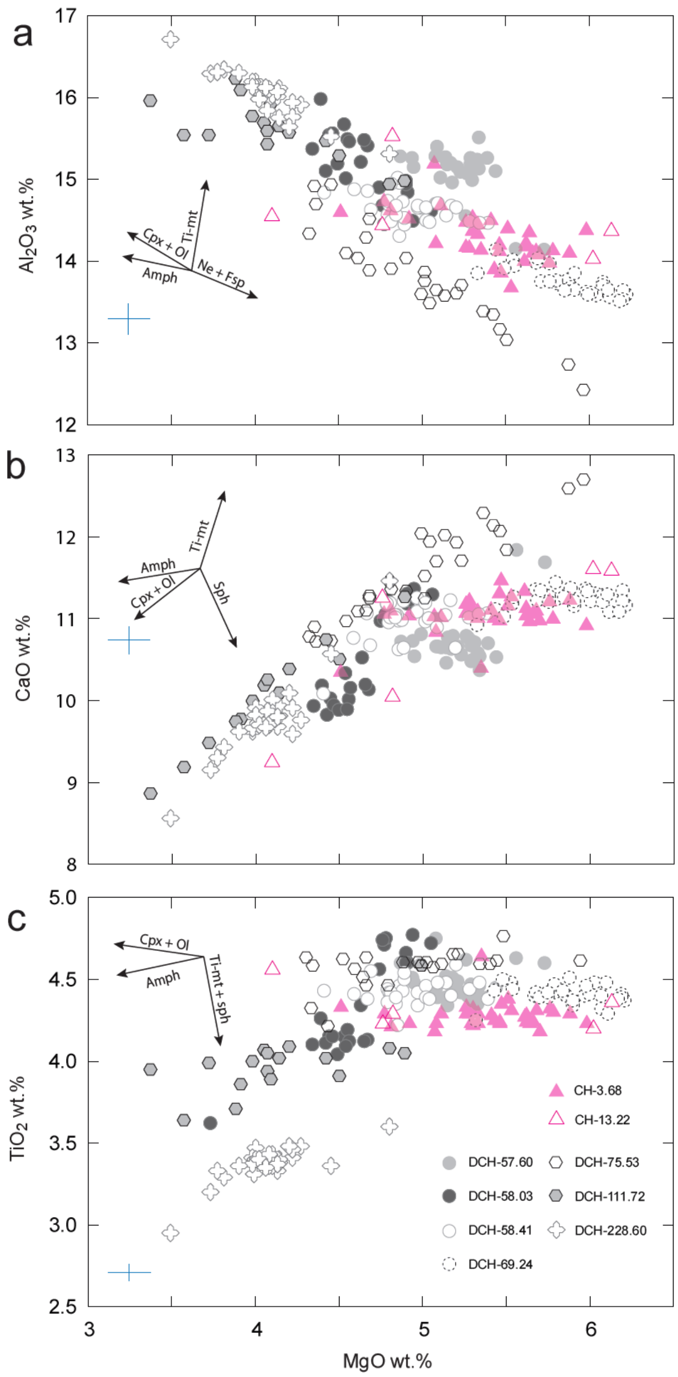

Fig. 4 *Single-shard major-element concentrations in the DeepCHALLA (grey symbols) and CHALLACEA (triangles) mafic tephras. Error bars (blue crosses, 2-sigma) are based on repeat analyses of the MPI-DING standard KL2-G, averaged across all analytical sessions. The trajectories of Al_2O_3 (a), CaO (b) and TiO_2 (c) concentration against MgO (all as wt. %) indicate magma evolution dominated by clinopyroxene and olivine fractionation; the vectors in each panel indicate the approximate crystallisation paths.*

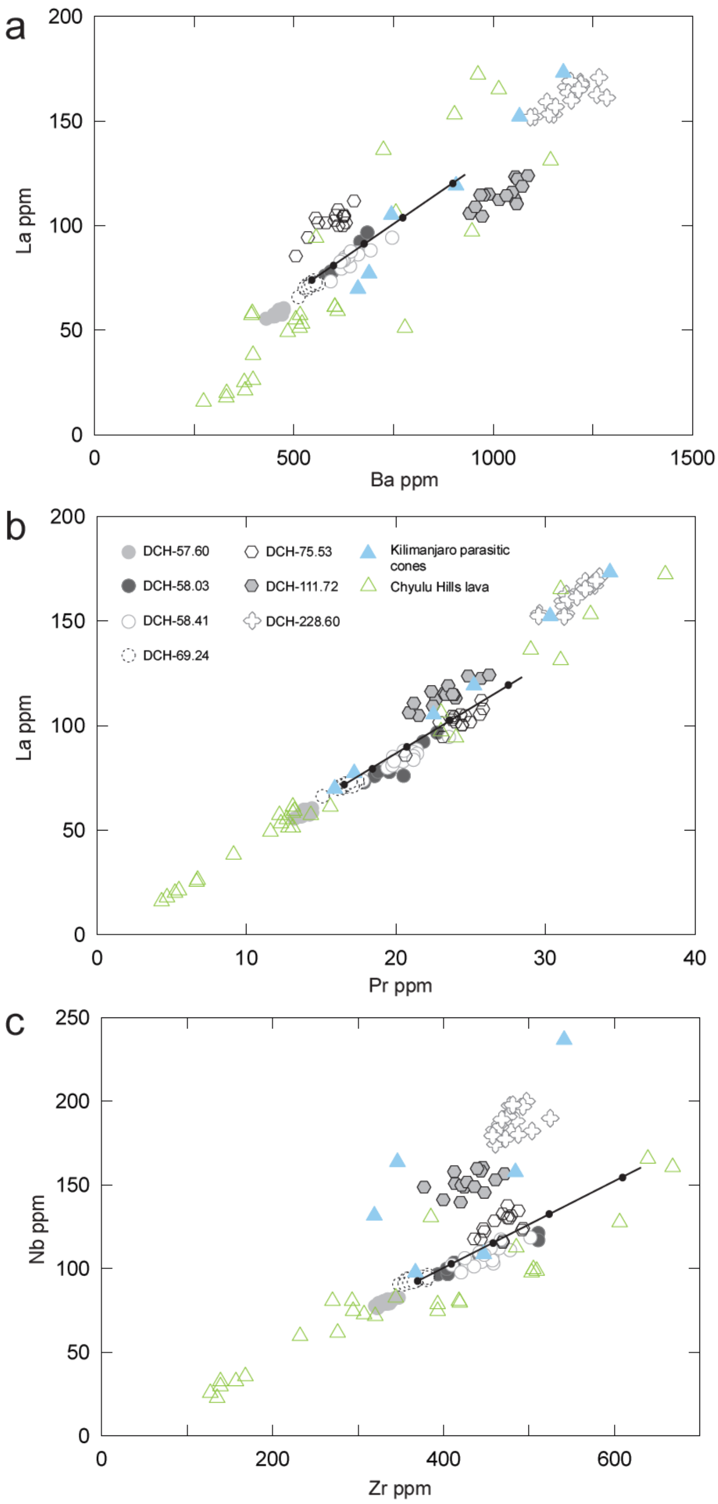

***Fig. 5** Relationships between concentrations of the incompatible elements La and Ba (a), La and Pr (b) and Nb and Zr (c) in single shards of the seven DeepCHALLA mafic tephras analysed (grey symbols), compared with those in lavas from Mt. Kilimanjaro 200-150 ka parasitic cones (blue closed triangle; whole-rock analyses by Nonnotte et al., 2011) and in lavas from the Chyulu Hills volcanic field (green open triangles; whole-rock analyses by Späth et al., 2001). Average 2-sigma errors, from repeat analyses of*

the MPI-DING standard StHs6-80G over two analytical sessions (10.5 ppm for Zr, 6.94 ppm for Nb, 36.6 ppm for Ba, 1.16 ppm for La and 0.357 ppm for Pr) are smaller than symbol sizes in this plot. Vectors (with 10% steps) show modelled simple fractional crystallisation of olivine and clinopyroxene using IgPet software (Carr and Gazel, 2017), with DCH-69.24 (the most mafic tephra) as the starting composition and using mineral-melt partition coefficients compiled by Späth et al. (2001).